I&EC research
Industrial & Engineering Chemistry Research

pubs.acs.org/IECR

Article

Synthesis and Evaluation of K-Promoted $Co_{3-x}Mg_xAl$-Oxides as Solid CO_2 Sorbents in the Sorption-Enhanced Water−Gas Shift (SEWGS) Reaction

Bjørnar Arstad,* Richard Blom, Silje F. Håkonsen, Joanna Pierchala, Paul Cobden, Fredrik Lundvall, Georgios N. Kalantzopoulos, David Wragg, Helmer Fjellvåg, and Anja O. Sjåstad

Cite This: *Ind. Eng. Chem. Res.* 2020, 59, 17837−17844

Read Online

ACCESS | Metrics & More | Article Recommendations | Supporting Information

ABSTRACT: Hydrogen is essential in a variety of large-scale chemical processes. As a carbon-free energy carrier, hydrogen has a potential for wide use within power production and transportation. However, most of the recent production methods involve the release of CO_2 as a by-product. Hence, decarbonization of hydrogen production is one step to reduce CO_2 emission into the Earth's atmosphere. Several process schemes have been suggested for low-carbon emission production of hydrogen. In this work, we show how to improve solid sorbents for the sorption-enhanced water−gas shift (SEWGS) process, which is a process that exploits a solid sorbent in the water−gas shift reactor to capture CO_2 in situ and drive the process toward an improved hydrogen yield. We report herein a series of $Co_xMg_{3-x}Al$ materials based on hydrotalcites, promoted with various loadings of K. The materials have been characterized by BET, XRD, and NMR and tested for their CO_2 adsorption performance in three adsorption−desorption cycles in a lab-scale fixed-bed reactor (20−22 bar, CO_2 + steam as reactant gas, and isothermal conditions at 375 and 400 °C). The most promising material was subjected to a long-term test (120 adsorption−desorption cycles at similar conditions). This test indicates that a K-promoted $Co_{1.5}Mg_{1.5}Al$ (22 wt % of added K_2CO_2 to the oxide) material has a higher cyclic capacity for CO_2 than standard reference cases. We have estimated that the volumetric capacity (in mol/L unit) of this sorbent will be 23−26% higher than a standard reference material at 400 °C and 30−39% higher at 375 °C. This would, in fixed-bed columns, lead to significant reduction in the needed column volumes in the final process and reduce costs.

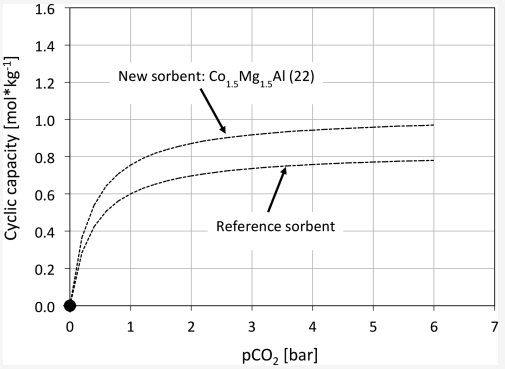

INTRODUCTION

The Intergovernmental Panel on Climate Change (IPCC) reports, "Human activities are estimated to have caused approximately 1.0 °C of global warming above pre-industrial levels, with a likely range of 0.8−1.2 °C".[1,2] With growing concern of negative consequences of climate changes, major efforts have been initiated to head for a low-emission and sustainable future. In addition to deploying technologies for providing energy from renewable sources, it is widely accepted that decarbonizing power production, transport, and industrial processes coupled with carbon capture and storage (CCS) is important to reach the necessary and ambitious goals.[3] At present, the most mature option for CCS from large point sources is CO_2 emission reduction by aqueous amine-based absorption processes.[4] A part of the solution for decarbonizing power and chemical productions is production of hydrogen from renewal energy sources, or via a process including CO_2 separation. In a conventional scheme for hydrogen production, natural gas is reformed and the produced synthesis gas is processed through two stages of water−gas shift units before the off-gas is cooled down to remove CO_2 by a process utilizing solvents (e.g., the Selexol or the Rectisol processes). However, other separation technologies for H_2 production are being developed, and these are, for example, based on membranes that can separate either H_2 or CO_2 from the gas streams,[5,6] chemical looping principles,[7] or sorbents that can be used to remove CO_2 in situ in the reactor in the so-called sorption-enhanced reactions (SERs).[8−11] In SER schemes, the high hydrogen yield is due to removal of the produced CO_2 by the sorbent (denoted MO in eqs 3−5 below), which drives the reactions toward products as explained by the Le Chatelier principle.

$$CH_4(g) + H_2O(g) \rightleftarrows 3H_2(g) + CO(g) \quad (1)$$

Received: May 7, 2020
Revised: August 27, 2020
Accepted: August 28, 2020
Published: August 28, 2020

$$CO(g) + H_2O(g) \rightleftarrows H_2(g) + CO_2(g) \quad (2)$$

$$MO(s) + CO_2(g) \rightleftarrows MCO_3(s) \quad (3)$$

$$CH_4(g) + 2H_2O(g) + MO(s) \rightleftarrows 4H_2(g) + MCO_3(s)\ SE - Reforming \quad (4)$$

$$CO(g) + H_2O(g) + MO(s) \rightleftarrows H_2(g) + MCO_3(s)\ SE - WGS \quad (5)$$

MO denotes a metal oxide that is transformed into a carbonate form by its reaction with CO_2. Ideally, an efficient carbon dioxide sorbent should be able to shift the reactions fully to the right side of the equations, leading to high yields of hydrogen and negligible concentrations of CO, CO_2, and methane (reactant feedstock). In all sorbent-based technologies, the sorbent has a certain absorption capacity and must be regenerated (back) into its initial state in order to be used again. Sorbent lifetime is thus a critical parameter for a successful process.

The work presented in this article is primarily relevant for the sorption-enhanced water−gas shift (SEWGS) process. The SEWGS process has already reached a technology readiness level suitable for upscaling to a pilot plant scale. However, it is highly desirable to improve the cyclic CO_2 absorption capacity of the sorbent as this will greatly improve the process economy.[12,13] Presently, the main sorbent type developed for the SEWGS technology is based on K-promoted hydrotalcites. The state-of-the-art sorbent exhibits stable performance for more than 2000 adsorption−desorption cycles.[14] Recent benchmarking of the SEWGS process integrated in both integrated gasification combined cycle (IGCC) and steelwork contexts has shown that the process has a relatively low specific energy need (SPECCA) compared with the state-of-the-art solvent-based technology.[15] A major factor that will reduce costs and implementation barriers is reduction of a process's footprint. For the SEWGS process, a major positive gain in these respects can be obtained by increasing the volumetric sorption capacity of the sorbent and/or reducing the cycle time used in the cyclic sorption/desorption process.

In 2008, synthesis, characterization, and sorption capacity of a series of Ca-, Mg-, and Co-containing Al-hydrotalcite-like compounds were reported and a remarkable CO_2 sorption capacity up to around 1.4 mol/kg, even without K-promotion, was observed.[16] However, only the CO_2 capacity of the first sorption cycle was reported and the pressure was only 1 atm. Considering that for sorption-based processes the operating pressure will likely be around 20 to 30 atm and that the major energy input is while regenerating the sorbent, we were motivated to further develop and assess some of these hydrotalcite-based sorbents in their K-promoted versions.

The present work reports synthesis, characterization, and testing of K-promoted sorbents based on $Co_xMg_{3-x}Al$ hydrotalcites at conditions relevant for the SEWGS process. We have chosen to focus our development on K-promoted materials as we have shown that without this promotion, the cyclic CO_2 capacity is not satisfactory.[17] Initial testing for three adsorption−desorption cycles were done at 21 bar, including the use of steam during both sorption and regeneration at 375 and 400 C°. From these initial tests, we could assess the general performance of the sorbents. The most stable material over these three cycles with the highest cyclic CO_2 capacity was made in a larger quantity and tested for 120 adsorption−desorption cycles.

EXPERIMENTAL SECTION

Material Preparation. The sorbents were prepared in two main stages. First, the base materials were made followed by K-promotion. The following chemical compounds from Sigma-Aldrich were used in the material preparation: $Al(NO_3)_3{\cdot}9H_2O$ (>98% pure), $Co(NO_3)_2{\cdot}6H_2O$ (>98% pure), $Mg(NO_3)_2$ (>99% pure), and K_2CO_3 (99%). Preparation of the base materials started with mixing of the metal salts into water in a glass beaker at room temperature. Separately, a NaOH solution was prepared. These two solutions were dripped during rigorous stirring into a beaker filled with water kept at 60 °C. The dripping rate of the salt solution was 2 mL/min, and the dripping rate of the NaOH solution was such that the pH was kept at about 10 ± 0.5. The pH was measured using a pH electrode. The mixture was then aged for 4 or 18 h at 60 or 75 °C, respectively, depending on the salt mixture. After cooling down, the precipitated product was washed four times with deionized water. Before calcination at 550 °C (overnight), the products were dried at 70 °C (overnight) and then at 120 °C for 2−3 h. Table 1 summarizes the main parameters of the base material synthesis.

Table 1. Summary of Synthesis Parameters for the Base Materials[a]

parameter	Co_3Al	$Co_{1.5}Mg_{1.5}Al$	Mg_3Al
pH during mixing	10 ± 0.5	10 ± 0.5	10 ± 0.5
temperature during mixing, °C	60	room temperature	60
aging time after mixing, h	4	18	4
aging temperature, °C	60	75	60
drying: 18−20 h + 2−3 h, °C	70 + 120	70 + 120	70 + 120
calcination temperature, °C	550	550	550

[a]Two batches were made of the $Co_{1.5}Mg_{1.5}Al$ material using the same synthesis conditions.

For all materials, we tried different aging times and temperatures. The reported materials were chosen from those that gave good XRD, BET, and pore volume data. The somewhat different conditions for the $Co_{1.5}Mg_{1.5}Al$ material was found to be most suited for this mixture of Mg and Co. After calcination at 550 °C, K_2CO_3 was deposited on the materials using the incipient wetness principle followed by heat treatment at 450 °C for 4 h in air. The amount of K_2CO_3 is reported so that the amount of K_2CO_3 plus the amount of base material constitutes 100%, that is, Mg_3Al (22) means 22 wt % K_2CO_3 and 78 wt % base material, Mg_3Al in this case. The final form is termed K-promoted materials.

Surface Area and Pore Volume. The specific surface areas (BET areas) of the powders were estimated from N_2 adsorption isotherms measured at 77 K on a BELSORP Mini instrument. Specific pore volumes were estimated from the same isotherms at p/p_o = 0.95. Estimated uncertainties of measured values are 5%.

X-Ray Diffraction. After material preparation but before deposition and promotion with K_2CO_3, in-house XRD measurements were carried out using a PANalytical Empyrean diffractometer. The system is equipped with a PIXcel3D solid-state detector. The measurements were carried out in reflection geometry using Cu Kα radiation of λ = 1.541874 Å and a step size of 0.013°. In addition, four samples (two base materials and their K-promoted forms) were measured using the Swiss-Norwegian Beamline BM01 at the European

https://dx.doi.org/10.1021/acs.iecr.0c02322
Ind. Eng. Chem. Res. 2020, 59, 17837−17844

Synchrotron Radiation Facility (ESRF), with a monochromatic synchrotron radiation of λ = 0.69264 Å. The beamline is fitted with a Huber goniometer and a Dectris Pilatus 2 M photon-counting pixel area detector.[18,19] The 2D diffraction data were converted to 1D PXRD diffraction patterns using Bubble and FIT2D programs.[17]

Nuclear Magnetic Resonance Spectroscopy. ^{27}Al MAS NMR spectra were acquired using a Bruker Avance III spectrometer operating at a magnetic field of 11.74 T at SINTEF, Oslo (Norway). The ^{27}Al resonance frequency at this field is 130.32 MHz. For the spectra, a 4 mm double resonance probe or a 3.2 mm triple resonance MAS probe was used. MAS rates were either 14 or 15 kHz. All NMR experiments were of the single-pulse type, that is, an initial delay (recovery) time followed by a pulse and an acquisition of the electric signal (free induction decay (FID)). For the ^{27}Al spectra, a total of 10,000 FIDs were recorded using a recovery time of 0.5 s. Before Fourier transformation of the averaged FIDs, zero filling and apodization were applied to improve line shape definitions and signal-to-noise ratios. The apodization was done by multiplying the accumulated FIDs with a decaying exponential window function with a processing line broadening (LB) factor of 150 Hz. All NMR spectra were adjusted by proper signal phasing and were baseline corrected.

Reactor Testing of Sorbent Performance. The prepared materials were tested for their CO_2 sorption performance at conditions relevant for the SEWGS process. The following protocol was applied for our performance screening (Figure 1).

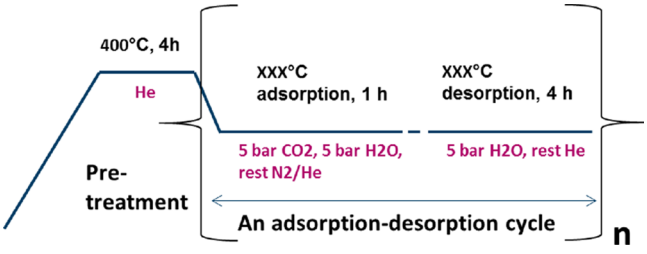

Figure 1. Schematic drawing of the fixed-bed screening protocol. XXX was set to either 375 or 400. The temperature was kept similar through each cycle for isothermal conditions.

The adsorption−desorption cycles were carried out in a high-throughput fixed-bed reactor system with four reactors in parallel. A sample amount of 200 μL was loaded in stainless steel reactors with a 4 mm inner diameter. The sample was pretreated in flowing He gas at 400 °C for 4 h (the heating ramp was 2 °C/min). After this, the sample was stabilized at reaction temperatures of 375 and 400 °C in He, and the 1 h adsorption step was carried out with the following gas mixture: 5 bar CO_2 and 5 bar steam, balanced with N_2 for a total pressure of 21.6 bar. CO_2 and N_2 were fed from a premix gas cylinder via separate Brooks mass flow controllers to each reactor. Steam was generated by feeding water through Bronkhorst liquid mass flow controllers, which was subsequently evaporated in a heated zone upstream of each reactor. Desorption of CO_2 (sorbent regeneration) was carried out for 4 h using 5 bar steam, balanced in He for a total pressure of 21.6 bar. The adsorption−desorption cycles were at isothermal and isobaric conditions.

Smooth transition between adsorption and desorption gases was ensured by crossover four-way valves located directly upstream of the reactors. Cyclic capacities were evaluated by integrating mass spectrometry (MS) data from online ProLab MS. The CO_2 concentration and breakthrough were measured following the m/z = 44 signal. After switching to the adsorption gas, the breakthrough of N_2 (m/z = 28) was used as a marker for the dead volume and time delay in the system.

After running multiple adsorption tests on the in-house prepared reference material and other prepared samples, the uncertainty in measurements, both in terms of reactor-to-reactor reproducibility and test-to-test reproducibility, was found to be ±0.1 mol/kg adsorbent.

One material from the screening experiments was tested for a total of 120 consecutive cycles in a fixed-bed column unit at TNO Energy Transition's (former ECN) facilities in Petten, Netherlands. These 120 cycles were split into three 40-cycle periods each with different process conditions, see below for details. The material chosen was based upon lab-scale fixed-bed testing. The experiments were conducted using a high-pressure multicolumn rig.[20] The inner diameter of the column was 9.2 mm. A sample material of 2.5 g was tested and compared with a material available from a commercial supplier, 20 wt % K_2CO_3 on Mg30 supplied by Sasol GMBH.[21] This commercial material is a standard reference material used for the SEWGS testing in this rig facility; hence, we decided to use that to compare with our new material. The samples were prepared to a sieve-fraction size of 212−450 μm. The columns are electrically heated, and experiments were carried out at a total pressure of 20 bar. During both adsorption and desorption, the reactors were each fed with 150 NmL min^{-1} of gas mixtures at 400 °C. Three different process settings were used, each for 40 cycles:

Setting 1: Adsorption: 25% CO_2, 25% H_2O, 50% N_2, Regeneration: 25% Ar, 25% H_2O, 50% N_2

Setting 2: Adsorption: 10% CO_2, 25% H_2O, 65% N_2, Regeneration: 10% Ar, 25% H_2O, 65% N_2

Setting 3: Adsorption: 3% CO_2, 25% H_2O, 72% N_2, Regeneration: 3% Ar, 25% H_2O, 72% N_2

The partial pressure of CO_2 was varied to investigate eventual CO_2 pressure-dependent material properties.

For every setting, the adsorption and regeneration characteristics were followed by measuring the outlet gas flow five times with regular intervals. The gas analysis was performed using a mass spectrometer measuring H_2 (m/z = 2), H_2O (m/z = 18), CO/N_2 (m/z = 28), Ar (m/z = 40), and CO_2 (m/z = 44). Cyclic capacities were calculated on the basis of half-height breakthrough.

Since the SEWGS process is anticipated to take place around 350−450 °C at a total pressure of 20−30 bar, our conditions for testing the new materials were not far from likely large-scale industrial operating conditions.

RESULTS AND DISCUSSION

Material Characterization. The BET surface and pore volume measurements are reported in Table 2 below, with literature values in parentheses.[14]

From the BET and pore volume data in Table 2, it is seen that the unpromoted base materials show a higher BET surface area than the K-promoted materials. The reference base material display, with a good margin, the highest surface and pore volume values, but these values decrease to the lowest after K-promotion.

https://dx.doi.org/10.1021/acs.iecr.0c02322
Ind. Eng. Chem. Res. 2020, 59, 17837−17844

Table 2. Specific Surface Areas (BET) and Pore Volumes from N_2 Adsorption Analyses at 77 K[a]

samples (K amount %)	BET, m^2/g	pore volume, cm^3/g
unpromoted base materials		
Mg_3Al	221(161)	1.20(0.40)
$Co_{1.5}Mg_{1.5}Al$, first batch	105(127)	0.83(0.45)
$Co_{1.5}Mg_{1.5}Al$, second batch	123(127)	0.63(0.45)
Co_3Al	91(96)	0.80(0.23)
K-promoted materials		
Mg_3Al (22) (reference in *screening* tests)	16	0.11
$Co_{1.5}Mg_{1.5}Al$ (5)	91	0.82
$Co_{1.5}Mg_{1.5}Al$ (10)	69	0.69
$Co_{1.5}Mg_{1.5}Al$ (15)	53	0.60
$Co_{1.5}Mg_{1.5}Al$ (22)	45	0.33
$Co_{1.5}Mg_{1.5}Al$ (30)	35	0.53
Co_3Al (22)	45	0.46

[a]Literature values in parentheses.[14]

XRD plots of the base materials are shown in Supporting Information Figure S1. These XRD diffractograms show that all the base materials have the same basic structure.

To confirm the anticipated structural stability of the Co-containing base materials after K-promotion, we performed high-quality XRD using synchrotron radiation before and after impregnation. These four diffractograms are shown in Figure 2 below.

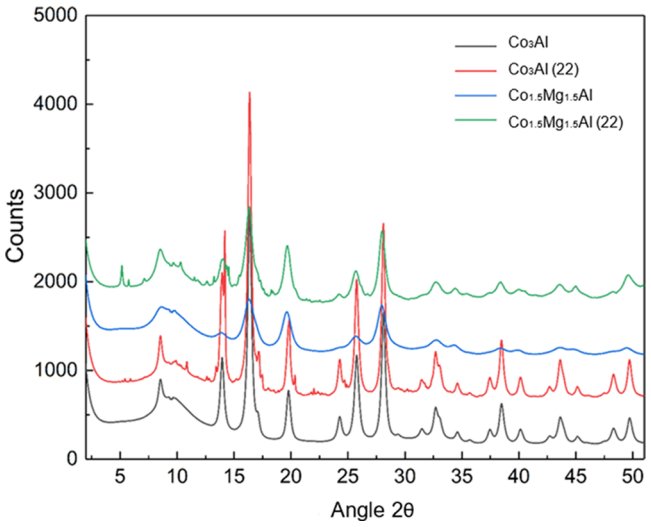

Figure 2. Synchrotron XRD data of the two types of Co-layered materials. The number in parenthesis in the legend indicates the amount of K_2CO_3 (wt %).

Most notable in Figure 2 is the rather similar overall features. However, the $Co_{1.5}Mg_{1.5}Al$ materials have broader peaks than the Co_3Al materials, suggesting a smaller crystallite size. The K-promoted samples show some extra small, sharp diffraction peaks, but the exact origin is not clear.

To gain further structural insights, we performed ^{27}Al NMR spectroscopy of selected samples, before and after K-promotion and after long-term testing. In Figure 3 below, we report ^{27}Al MAS NMR spectra of the Mg_3Al base material after drying at 120 °C, after calcination at 550 °C, and after K-promotion and heat treatment at 450 °C (from top to bottom, respectively). The motivation for the NMR data presented in Figure 3 is to obtain information on the base reference material and thus be in a better position to understand the Co-containing materials.

After synthesis and drying at 120 °C, the Al spectrum (Figure 3 top) shows one strong peak at 11 ppm. Since this material consists of brucite-like sheets with edge-shared octahedra of hydroxy-coordinated cations, and Al octahedrally coordinated to O-atoms is known to have a chemical shift close to 0 ppm, this peak is assigned to Al in the brucite sheets. In addition, there is a small broad skewed peak with maximum height at a chemical shift of 75 ppm that can be assigned to tetrahedral coordinated Al.[22] Heat treatment at 550 °C induces major changes. During such a temperature treatment, major dehydroxylation takes place and a large fraction of octahedral Al becomes tetrahedrally coordinated. This gives rise to the skew peak with a maximum at 75 ppm. Peak-shape skewing toward lower frequencies is due to distribution of quadrupolar coupling constants of the Al nuclei. After K-promotion and heat treatment, it appears that a higher degree of tetrahedral Al is present in the sample, compared with that before K-promotion.

Furthermore, we carried out ^{27}Al MAS NMR spectroscopy studies of the $Co_{1.5}Mg_{1.5}Al$ material to investigate changes in the Al environments when parts of Mg were exchanged with Co. The ^{27}Al MAS spectra of the $Co_{1.5}Mg_{1.5}Al$ material and the K-promoted form are shown in Figure 4.

In the top left part of Figure 4, the ^{27}Al spectrum of $Co_{1.5}Mg_{1.5}Al$ is shown after it has been heated at 550 °C. The two peaks marked with asterisks are from the central transitions. The peaks are located around 9 and 70 ppm, indicating that there are Al nuclei in both an octahedral environment (around 0−10 ppm) and a tetrahedral environment (60−70 ppm) in the sample. After K-promotion of the $Co_{1.5}Mg_{1.5}Al$ material, the spectrum changes quite significantly (in contrast to what is seen in Figure 3 before and after K-promotion of the Mg_3Al material). We can see that K-promotion of $Co_{1.5}Mg_{1.5}Al$ has resulted in a large new peak centered around 5 ppm (indicated with an arrow). By superimposing the two spectra (Figure 4 right), we can see that the two original peaks are most likely still present, but there is a new intense sharp peak. The left shoulder of this intense peak appears to be the original peak present before K-promotion. Since no Al is added during the K-promotion, a change must have taken place in the material such that more Al nuclei have become "NMR visible." One explanation might be that reduction of quadrupolar couplings of the Al nuclei results in stronger peak intensity. The possible loss of intensity in peaks from the nuclei with very strong quadrupolar couplings is a well-known effect. In such cases, the peaks broaden and turn "invisible" due to inefficient excitation. However, at the field strength we have applied in this work, the effects should not be too strong since the effects are inversely proportional to the magnetic field strength. In addition, we know that most or all Al nuclei in our materials are octahedrally coordinated with relatively weak quadrupolar couplings. Hence, we must seek another explanation than reduction of quadrupolar couplings of Al after K-promotion. A second suggestion comes from a report that the mineral dawsonite is formed in situ in alkali metal-promoted alumina.[23] The original Al peaks should then also change intensity as well. By comparing ^{27}Al NMR spectra of the K-promoted $Co_{1.5}Mg_{1.5}Al$ material with K−dawsonite reported in the literature, we can see a resemblance, see Supporting Information Figure S2, albeit not completely.[24]

https://dx.doi.org/10.1021/acs.iecr.0c02322
Ind. Eng. Chem. Res. 2020, 59, 17837−17844

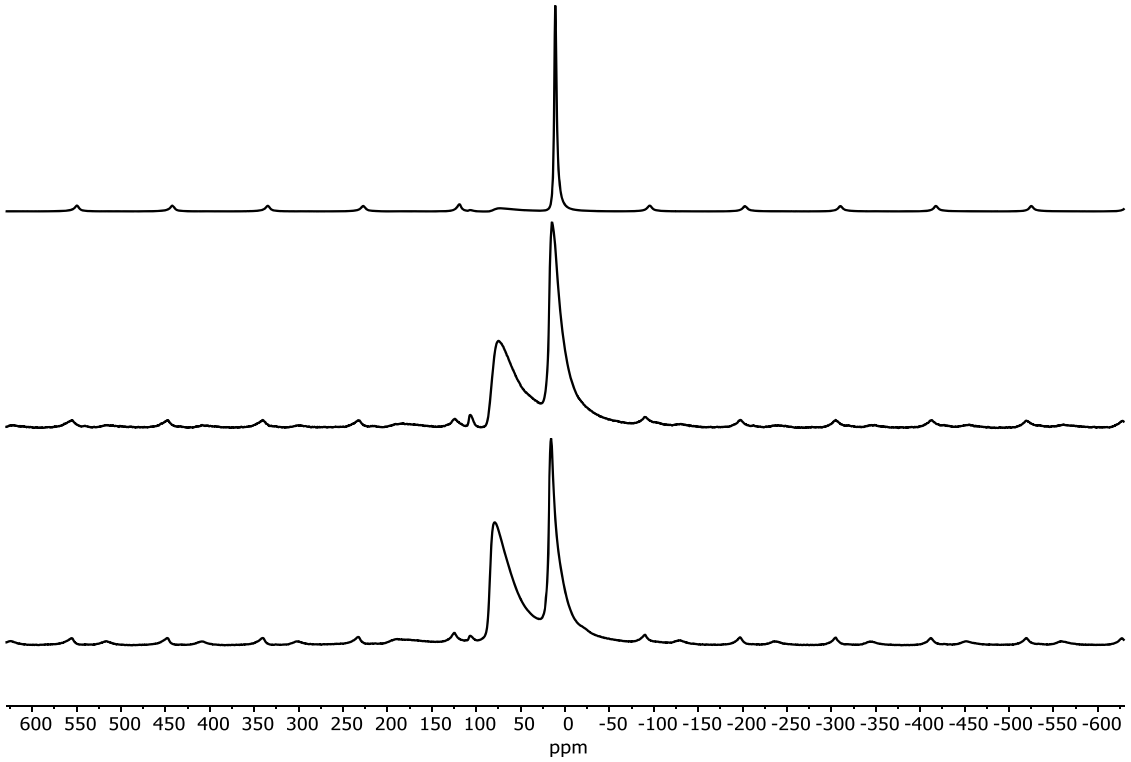

Figure 3. ^{27}Al MAS NMR spectra (4 mm MAS probe) of the Mg_3Al base material after drying at 120 °C (top), after calcination at 550 °C (middle), and after K-promotion with heat treatment at 450 °C (bottom).

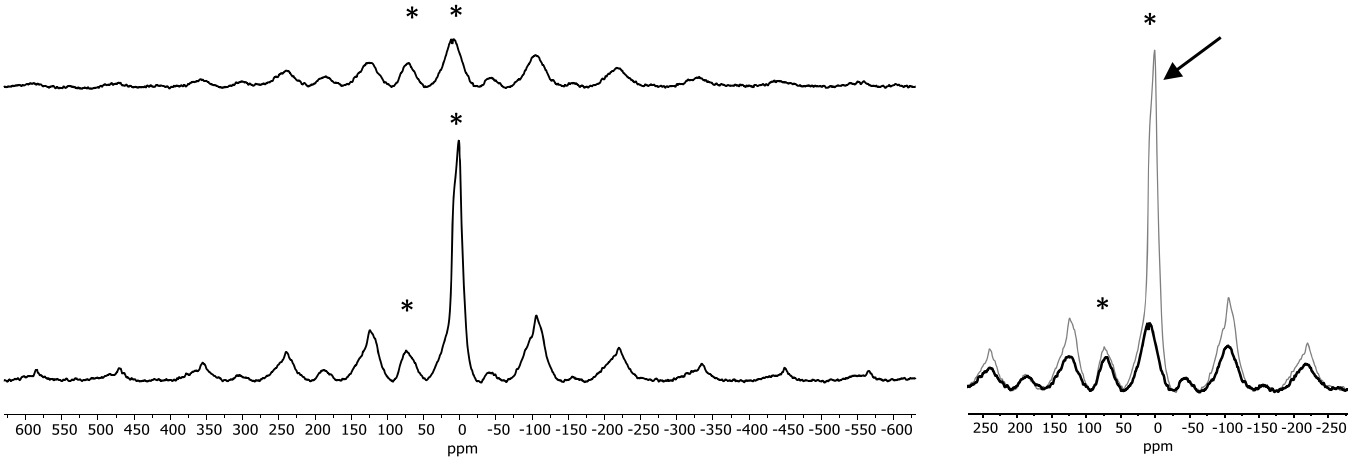

Figure 4. Left: ^{27}Al solid-state NMR (3.2 mm MAS probe) of $Co_{1.5}Mg_{1.5}Al$ after heat treatment at 550 °C (top) and after K-promotion (lower). The asterisks mark the central transition peaks. Unmarked peaks are spinning sidebands from the satellite transitions. Right: Superimposed spectra to highlight the presence of a new Al peak in the K-promoted sample. The new peak is indicated with the arrow. Note that there is no scaling of the spectra, and hence the intensity increase after K-promotion is, at least qualitatively, comparable.

The maxima in these samples are actually at the same chemical shift, but curve fitting including models for quadrupolar couplings has so far not given any conclusive evidence for similar phases in the two materials. A third possible explanation to our observation is that promotion of the base material with K decouples Al from the influence of paramagnetic Co(II). K may form bonds with oxygen atoms and quench the influence of paramagnetic Co(II) on the ^{27}Al nuclei that travel through sigma bonds. Materials with paramagnetic centers, for example, Co(II) in our case, are susceptible to strong interactions that complicate NMR analyses. Paramagnetic ions are themselves not observable by NMR spectroscopy but influence their nearby nuclei. The main effects that an electronic paramagnetic center may lead to are peak position shifts, line broadening, and enhanced relaxation rates of nearby nuclei. The interactions that results in these observations are due to through-space electron-nuclei dipole−dipole interactions, or localized electron density from the paramagnetic center, or the conducting electrons in a metal, at the nuclei in question. The last interactions are called the Fermi contact interaction. Two critical factors relevant for NMR analyses of such systems are the distance between the observed nuclei and the paramagnetic center or whether the paramagnetic center is in a bonding network with the nearby

https://dx.doi.org/10.1021/acs.iecr.0c02322
Ind. Eng. Chem. Res. 2020, 59, 17837−17844

atoms. If the paramagnetic ion is neither covalently bonded nor strongly coordinated with the atoms studied with NMR, the influence through the Fermi contact is very weak or absent. In these cases, only an enhanced relaxation rate is observed. However, by strong enough interactions at proper conditions, the lifetime of the coherence giving rise to the signals is so short that the Fourier-transformed signals end up as peaks broadened into nothing. Recently, it was demonstrated that there is an increasing influence of paramagnetic Eu^{2+} when doped into a series of SrH_2 ($Sr_{1-x}Eu_xH_2$). From ^1H MAS NMR, it was shown that the influence of paramagnetic Eu^{2+} ions on nearby ^1H nuclei leads to a sphere with a "wipe-out radius" of 1.7 nm (which is about 10 typical Al−O/Si−O covalent bond lengths).[25] Even when paramagnetic centers impose complications in NMR experiments, it is often possible to successfully conduct useful NMR experiments on materials with paramagnetic centers, as summarized in a review by Grey and Dupré.[26] In fact, the interactions that complicate the NMR spectra also lead to more parameters to work with when characterizing the materials as the presence or absence of peak-shape distortions is the key to understanding the systems. In our case, this third explanation appears to best fit with our observations. The introduced K will influence the oxide material, and from our NMR data, it appears that K influences the oxide so that otherwise "invisible" Al due to electronic paramagnetism becomes visible.

CO_2 Adsorption Performance Testing. After preparation and characterization, each material was tested for three adsorption−desorption cycles to assess the most promising sorbent at two different temperatures. A possible objection to our three-cycle tests is that they do not give long-term stability and only give indications of the initial cyclic capacity. However, we know from extensive testing that one can indicate the general cyclic capacity of these materials with satisfactory accuracy after a few cycles. By contrast, CaO-based solid sorbents decline in performance almost from the first run, and the long-term residual capacity must be assessed when considering working capacity.[27] Thus, our main selection criterion for assessing the long-term residual capacity was based on cyclic capacity and resistance to deactivation during these three cycles. For the screening tests, we used an in-house-prepared material (Mg_3Al (22)) as reference and standard for error estimation. Table 3 gives a summary of the most relevant and important lab-scale screening tests.

There are several points to note from the data in Table 3. The Co_3Al (22) material has a much lower cyclic capacity than the other two materials with the same amount of K, and there is an increase in capacity when the K amount is increased in the $Co_{1.5}Mg_{1.5}Al$ series. Due to the small error margins (vide supra), we are able to state that the two highly loaded K-promoted materials ($Co_{1.5}Mg_{1.5}Al$ (22) and $Co_{1.5}Mg_{1.5}Al$ (30)) show a higher cyclic capacity (about 10−12% at 400 °C and 17−25% at 375 °C) compared with the state-of-the-art reference.

Table 3. Summary of CO_2 Uptake (in mol/kg) for the Various Materials at 375 and 400 °C in Three Consecutive Adsorption−Desorption Cycles

	cycle # at 375 °C			cycle # at 400 °C		
sample name (prom. %)	1	2	3	1	2	3
reference Mg_3Al (22)	1.5	1.8	1.9	1.6	1.7	1.7
$Co_{1.5}Mg_{1.5}Al$ (5)	1.1	1.0	1.0	0.9	0.9	1.0
$Co_{1.5}Mg_{1.5}Al$ (10)	1.3	1.2	1.2	1.0	1.1	1.1
$Co_{1.5}Mg_{1.5}Al$ (15)	1.3	1.5	1.5	1.3	1.3	1.3
$Co_{1.5}Mg_{1.5}Al$ (22)	1.7	2.0	2.0	1.9	1.8	1.8
$Co_{1.5}Mg_{1.5}Al$ (30)	1.4	1.8	2.0	1.6	1.8	1.8
Co_3Al (22)	0.4	0.5	0.5	0.4	0.5	0.5

A question that arises from the data reported herein is why K promotes CO_2 sorption in some of these materials. It has been reported that the dawsonite phase is formed in situ under SEWGS conditions,[21] and together with our recently published work,[22] we can suggest that maybe a new phase or domain of reactive sites is formed after the oxide reaction with K that might be, or resembles, dawsonite in some way. The ^{27}Al NMR data shown above also indicated new structural components after K-promotion. Furthermore, it appears that Mg is important because the sample without Mg did not have any appreciable CO_2 uptake after K promotion. In sorbents relying on physisorption of CO_2, that is, where adsorption is mainly driven by van der Waal's forces between CO_2 and the structure itself, one typically observes an increased uptake with an increased specific surface area. However, in our case, the surface area is strongly reduced after K promotion, but CO_2 uptake increases significantly. This again hints to the importance of a likely new phase, still to be characterized in detail.

For further long-term testing, we chose $Co_{1.5}Mg_{1.5}Al$ (22). Data from this test are shown in Figure 5. Note that the reference sample reported in Figure 5 is from a commercial producer and is not the same as reported in Table 3.

From the left graph, one can see that the new material outperformed the reference with regard to uptake capacity at the applied conditions. Furthermore, from the right graph, we can see that the performance is rather stable and no strong deactivation takes place. The different levels are due to different partial pressures of CO_2 in the feed gas. A relevant question is if the material has experienced any changes even if the performance in the test rig is quite stable. From BET and pore volume measurements of the used material (Table 4), it is clear that the BET surface and the pore volume has decreased significantly during the 120 adsorption−desorption cycles.

Evaluation of possible improvement in the SEWGS process using a sorbent with increased CO_2 capacity was done for the $Co_{1.5}Mg_{1.5}Al$ (22) material by assuming that the material can be compacted/shaped/pelletized in a similar manner as the reference. Based on this, we estimated the volumetric capacity (in mol/L unit) of the sorbents. Since the ionic radii of four-coordinated Co^{2+} and Mg^{2+} in the crystal are similar, 0.58 and 0.57 Å, respectively,[28] we estimate the crystal density of the mixed Co/Mg sorbent ($Co_{1.5}Mg_{1.5}Al$) to be 13−14% higher than that of the reference sorbent (Mg_3Al). Therefore, the volumetric capacity (in mol/L unit) of the mixed sorbent should be 23−26% higher than the reference at 400 °C and 30−39% higher at 375 °C. This would, in fixed-bed columns, lead to significant reduction in required column volumes in the final process.

CONCLUSIONS

In this work, we have reported synthesis and characterization of a series of K-promoted Mg_3Al, $Co_{1.5}Mg_{1.5}Al$, and Co_3Al oxides and tested their cyclic CO_2 adsorption capacity at conditions relevant for the SEWGS process. From lab reactor screening tests, we found that the $Co_{1.5}Mg_{1.5}Al$ (22) material appeared to have better cyclic CO_2 capacity than our reference

https://dx.doi.org/10.1021/acs.iecr.0c02322
Ind. Eng. Chem. Res. 2020, 59, 17837−17844

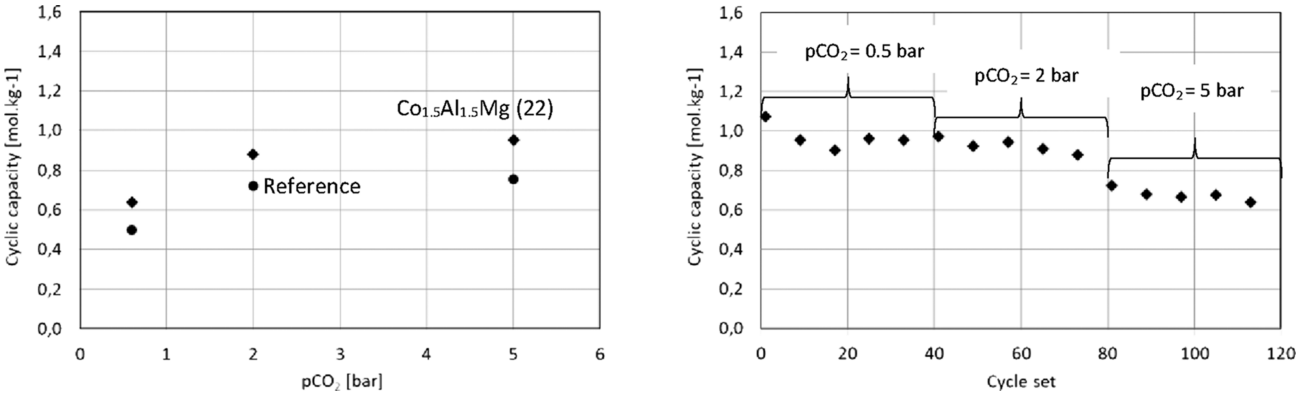

Figure 5. Data from multicycle testing of the $Co_{1.5}Mg_{1.5}Al$ (22) sample. Both adsorption and desorption are at 400 °C. Partial pressures of CO_2 were 0.5, 2, and 5 bar in the three different applied conditions. Left: Graph showing the uptake capacity at three different partial pressures of CO_2 for both our sample and the reference sample. Right: Performance over multiple cycles at three different partial pressures of CO_2.

Table 4. Specific Surface Areas (BET) and Pore Volumes from N_2 Adsorption Analyses at 77 K for the Samples Tested for 120 Cycles

samples	BET, m^2/g	pore volume, cm^3/g
$Co_{1.5}Mg_{1.5}Al$ (22), unused[a]	40	0.25(2)
$Co_{1.5}Mg_{1.5}Al$ (22) after 120 cycles	17	0.14

[a]Note that the values for the unused sample reported here are slightly different from the similar batch reported in Table 2. These differences should be attributed to normal variations in material preparation.

material. The $Co_{1.5}Mg_{1.5}Al$ (22) material was further tested for long-term capacity and stability through 120 adsorption cycles. Through these 120 adsorption−desorption cycles, the material shows improved performance compared with the state-of-the-art reference case.

Estimated volumetric capacity (in mol/L unit) of the new $Co_{1.5}Mg_{1.5}Al$ (22) sorbent is 23−26% higher than the reference at 400 °C and 30−39% higher at 375 °C, which would, in fixed-bed columns, lead to significant reduction in needed column volumes in the final process.

The improvement in cyclic CO_2 capacity of the new sorbent relative to state-of-the-art sorbents by manipulating the cation composition indicates that one should be able to fine-tune sorbent properties further and make the SEWGS process an even stronger competitor to other hydrogen-producing processes with CO_2 capture.

■ ASSOCIATED CONTENT

Supporting Information

The Supporting Information is available free of charge at https://pubs.acs.org/doi/10.1021/acs.iecr.0c02322.

Stacked plot of XRD diffractograms of all the base materials and ^{27}Al MAS NMR spectra of K−dawsonite (thin line)[21] and the K-promoted Co1.5 Mg1.5Al sample from this work. (PDF).

■ AUTHOR INFORMATION

Corresponding Author

Bjørnar Arstad − *SINTEF Industry, 0373 Oslo, Norway;* orcid.org/0000-0003-0398-786X; Email: bjornar.arstad@sintef.no

Authors

Richard Blom − *SINTEF Industry, 0373 Oslo, Norway;* orcid.org/0000-0001-8675-0774

Silje F. Håkonsen − *SINTEF Industry, 0373 Oslo, Norway*

Joanna Pierchala − *SINTEF Industry, 0373 Oslo, Norway*

Paul Cobden − *TNO Energy Transition, 1755 LE Petten, Netherlands*

Fredrik Lundvall − *Centre for Materials Science and Nanotechnology (SMN), Department of Chemistry, University of Oslo, Oslo N-0371, Norway*

Georgios N. Kalantzopoulos − *Centre for Materials Science and Nanotechnology (SMN), Department of Chemistry, University of Oslo, Oslo N-0371, Norway*

David Wragg − *Centre for Materials Science and Nanotechnology (SMN), Department of Chemistry, University of Oslo, Oslo N-0371, Norway*

Helmer Fjellvåg − *Centre for Materials Science and Nanotechnology (SMN), Department of Chemistry, University of Oslo, Oslo N-0371, Norway*

Anja O. Sjåstad − *Centre for Materials Science and Nanotechnology (SMN), Department of Chemistry, University of Oslo, Oslo N-0371, Norway*

Complete contact information is available at: https://pubs.acs.org/10.1021/acs.iecr.0c02322

Notes

The authors declare no competing financial interest.

■ ACKNOWLEDGMENTS

The authors acknowledge the support from the Research Council of Norway (project #243736) and thank Aud I. Spjelkavik (SINTEF) for material preparation/BET and pore volume measurements and Anna Lind (SINTEF) for XRD measurements.

■ REFERENCES

(1) IPCC, 2018: Summary for Policymakers. In *Global warming of 1.5°C. An IPCC Special Report on the impacts of global warming of 1.5°C above pre-industrial levels and related global greenhouse gas emission pathways, in the context of strengthening the global response to the threat of climate change, sustainable development, and efforts to eradicate poverty*; Masson-Delmotte, V.; Zhai, P.; Pörtner, H.-O.; Roberts, D.; Skea, J.; Shukla, P. R.; Pirani, A.; Moufouma-Okia, W.; Péan, C.; Pidcock, R.; Connors, S.; Matthews, J. B. R.; Chen, Y.; Zhou, X.; Gomis, M. I.; Lonnoy, E.; Maycock, T.; Tignor, M.;

https://dx.doi.org/10.1021/acs.iecr.0c02322
Ind. Eng. Chem. Res. 2020, 59, 17837−17844

Waterfield, T., Eds.; World Meteorological Organization: Geneva, Switzerland, 32 pp.
(2) Schlömer, S.; Bruckner, T.; Fulton, L.; Hertwich, E.; McKinnon, A.; Perczyk, D.; Roy, J.; Schaeffer, R.; Sims, R.; Smith, P.; Wiser, R. Annex III: Technology-specific cost and performance parameters. In *Climate Change 2014: Mitigation of Climate Change. Contribution of Working Group III to the Fifth Assessment Report of the Intergovernmental Panel on Climate Change*; Edenhofer, O.; Pichs-Madruga, R.; Sokona, Y.; Farahani, E.; Kadner, S.; Seyboth, K.; Adler, A.; Baum, I.; Brunner, S.; Eickemeier, P.; Kriemann, B.; Savolainen, J.; Schlömer, S.; von Stechow, C.; Zwickel, T.; Minx, J.C., Eds.; Cambridge University Press: Cambridge, United Kingdom and New York, NY, USA, 2014.
(3) Boot-Handford, M. E.; Abanades, J. C.; Anthony, E. J.; Blunt, M. J.; Brandani, S.; Mac Dowell, N.; Fernández, J. R.; Ferrari, M. C.; Gross, R.; Hallett, J. P.; Haszeldine, R. S.; Heptonstall, P.; Lyngfelt, A.; Makuch, Z.; Mangano, E.; Porter, R. T. J.; Pourkashanian, M.; Rochelle, G. T.; Shah, N.; Yao, J. G.; Fennell, P. S. Carbon capture and storage update. *Energy Environ. Sci.* **2014**, *7*, 130−189.
(4) Rochelle, G. T. Amine Scrubbing for CO_2 Capture. *Science* **2009**, *325*, 1652−1654.
(5) Peters, T. A.; Stange, M.; Sunding, M. F.; Bredesen, R. Stability investigation of micro-configured Pd-Ag membrane modules - Effect of operating temperature and pressure. *Int. J. Hydrogen Energy* **2015**, *40*, 3497−3505.
(6) He, X.; Lindbråthen, A.; Kim, T. J.; Hägg, M. B. Pilot testing on fixed-site-carrier membranes for CO_2 capture from flue gas. *Int. J. Greenhouse Gas Control* **2017**, *64*, 323−332.
(7) Dou, B.; Zhang, H.; Cui, G.; Wang, Z.; Jiang, B.; Wang, K.; Chen, H.; Xu, Y. Hydrogen production and reduction of Ni-based oxygen carriers during chemical looping steam reforming of ethanol in a fixed-bed reactor. *Int. J. Hydrogen Energy* **2017**, *42*, 26217−26230.
(8) Harrison, D. P. Sorption-Enhanced Hydrogen Production: A Review. *Ind. Eng. Chem. Res.* **2008**, *47*, 6486−6501.
(9) Arstad, B.; Prostak, J.; Blom, R. Continuous hydrogen production by sorption enhanced steam methane reforming (SE-SMR) in a circulating fluidized bed reactor: Sorbent to catalyst ratio dependencies. *Chem. Eng. J.* **2012**, *189-190*, 413−421.
(10) Jansen, D.; van Selow, E.; Cobden, P.; Manzolini, G.; Macchi, E.; Gazzani, M.; Blom, R.; Henriksen, P. P.; Beavis, R.; Wright, A. SEWGS Technology is Now Ready for Scale-up! *Energy Procedia* **2013**, *37*, 2265−2273.
(11) Dou, B.; Zhang, H.; Cui, G.; Wang, Z.; Jiang, B.; Wang, K.; Chen, H.; Xu, Y. Hydrogen production by sorption-enhanced chemical looping steam reforming of ethanol in an alternating fixed-bed reactor: Sorbent to catalyst ratio dependencies. *Energy Convers. Manage.* **2018**, *155*, 243−252.
(12) Manzolini, G.; Macchi, E.; Gazzani, M. CO_2 capture in natural gas combined cycle with SEWGS. Part B: Economic assessment. *Int. J. Greenhouse Gas Control* **2013**, *12*, 502−509.
(13) Gazzani, M.; Macchi, E.; Manzolini, G. CO_2 capture in integrated gasification combined cycle with SEWGS − Part A: Thermodynamic performances. *Fuel* **2013**, *105*, 206−219.
(14) van Selow, E. R.; Cobden, P. D.; Wright, A. D.; van den Brink, R. W.; Jansen, D. Improved sorbent for the sorption-enhanced water-gas shift process. *Energy Procedia* **2011**, *4*, 1090−1095.
(15) Gazzani, M.; Romano, M. C.; Manzolini, G. CO_2 capture in integrated steelworks by commercial-ready technologies and SEWGS process *Int. J. Greenhouse Gas Control* **2015**, *41*, 249−267.
(16) Wang, X. P.; Yu, J. J.; Cheng, J.; Hao, Z. P.; Xu, Z. P. High-temperature adsorption of carbon dioxide on mixed oxides derived from hydrotalcite-like compounds *Environ. Sci. Technol.* **2008**, *42*, 614−618.
(17) Lundvall, F.; Kalantzopoulos, G.; Wragg, D. S.; Arstad, B.; Blom, R.; Sjåstad, A. O.; Fjellvåg, H. Thermogravimetric analysis − a viable method for screening novel materials for the sorbent enhanced water-gas shift process. *En. Proc.* **2017**, *114*, 2294−2303.
(18) Broennimann, C. The PILATUS detectors: Hybrid pixel detectors for synchrotron and industrial applications. *Acta Cryst.* **2008**, *A64*, C162.
(19) Dyadkin, V.; Pattison, P.; Dmitriev, V.; Chernyshov, D. A new multipurpose diffractometer PILATUS@ SNBL. *J. Synchrotron Radiat.* **2016**, *23*, 825−829.
(20) van Dijk, H. A. J.; Cohen, D.; Hakeem, A. A.; Makkee, M.; Damen, K. Validation of a water−gas shift reactor model based on a commercial FeCr catalyst for pre-combustion CO_2 capture in an IGCC power plant. *Int. J. Greenhouse Gas Control* **2014**, *29*, 82−91.
(21) Boon, J.; Cobden, P. D.; van Dijk, H. A. J.; Hoogland, C.; van Selow, E. R.; van Sint Annaland, M. Isotherm model for high-temperature, high-pressure adsorption of CO_2 and H_2O on K-promoted hydrotalcite. *Chem. Eng. J.* **2014**, *248*, 406−414.
(22) Sjåstad, A. O.; Andersen, N. H.; Vajeeston, P.; Karthikeyan, J.; Arstad, B.; Karlsson, A.; Fjellvåg, H. On the Thermal Stability and Structures of Layered Double Hydroxides $Mg_{1-x}Al_x(OH)_2(NO_3)_x \cdot mH_2O$ ($0.18 \leq x \leq 0.38$). *Eur. J. Inorg. Chem.* **2015**, *2015*, 1775−1788.
(23) Walspurger, S.; Cobden, P. D.; Haije, W. G.; Westerwaal, R.; Elzinga, G. D.; Safonova, O. V. In Situ XRD Detection of Reversible Dawsonite Formation on Alkali Promoted Alumina: A Cheap Sorbent for CO_2 Capture. *Eur. J. Inorg. Chem.* **2010**, 2461−2464.
(24) Lundvall, F.; Kalantzopoulos, G.; Wragg, D. S.; Arstad, B.; Blom, R.; Sjåstad, A. O.; Fjellvåg, H. Characterization and evaluation of synthetic Dawsonites as CO_2 sorbents. *Fuel* **2019**, *236*, 747−754.
(25) Li, W.; Celinski, V.; Weber, J.; Kunkel, N.; Kohlmann, H.; Schmedt auf der Günne, J. Homogeneity of Doping with Paramagnetic Ions by NMR. *Phys. Chem. Chem. Phys.* **2016**, *18*, 9752−9757.
(26) Grey, C. P.; Dupré, N. NMR Studies of Cathode Materials for Lithium-Ion Rechargeable Batteries. *Chem. Rev.* **2004**, *104*, 4493−4512.
(27) Lind, A.; Thorshaug, K.; Andreassen, K. A.; Blom, R.; Arstad, B. The Role of Water during CO_2 Adsorption by Ca-Based Sorbents at High Temperature. *Ind. Eng. Chem. Res.* **2018**, *57*, 2829−2837.
(28) Shannon, R. D. Revised Effective Ionic Radii and Systematic Studies of Interatomic Distances in Halides and Chalcogenides. *Acta Cryst.* **1976**, *32*, 751−767.

https://dx.doi.org/10.1021/acs.iecr.0c02322
Ind. Eng. Chem. Res. 2020, 59, 17837−17844